ELSEVIER

Contents lists available at ScienceDirect

# International Journal of Heat and Mass Transfer

journal homepage: www.elsevier.com/locate/hmt



# Structural-material-operational performance relationship for pool boiling on enhanced surfaces using deep neural network model



Sadaf Mehdi<sup>a</sup>, Saideep Nannapaneni<sup>b</sup>, Gisuk Hwang<sup>a,\*</sup>

- <sup>a</sup> Department of Mechanical Engineering, Wichita State University, Wichita, KS 67260, USA
- <sup>b</sup> Department of Industrial, Systems, and Manufacturing Engineering, Wichita State University, Wichita, KS 67260, USA

#### ARTICLE INFO

Article history: Received 7 July 2022 Revised 17 August 2022 Accepted 28 August 2022

Keywords: Heat transfer coefficient Reentrant cavity Machine learning

#### ABSTRACT

An accurate predictive model of the enhanced pool boiling heat transfer on various surface modifications is essential to operate the pool boiling and design the optimal surface designs. However, the existing predictive models generally predict the enhanced pool boiling heat transfer on various surfaces with very large errors as high as  $\pm 50\%$ , mainly due to the complex nature of the pool boiling processes. In this study, we unlock the complex relations among four geometrical, nine thermophysical properties, and two operational conditions to accurately predict the Heat Transfer Coefficient (HTC) on the enhanced surfaces using an optimized Deep Neural Network (DNN) model. The six dimensionless numbers are identified based on geometries, operation conditions, and thermophysical properties, which are used as input parameters for the DNN model for the first time. This results in the Mean Absolute Percentage Error (MAPE) below 5%, compared to the existing empirical correlations having 5.04-45.37% MAPE on the selected 1256 data points. Also, the developed DNN model outperforms the prediction accuracy of the existing correlation for the data in much different experimental conditions, showing the 20% MAPE for the pre-trained DNN model (without additional training) and 38% MAPE for the existing correlation. Moreover, the sensitivity analysis was performed to identify the key dimensionless parameters for the HTC on the enhanced surfaces. The developed DNN model with the dimensionless parameters shed light on understanding the complex pool boiling process on the enhanced surfaces.

© 2022 Elsevier Ltd. All rights reserved.

#### 1. Introduction

The nucleate boiling offers a large heat transfer with a very small temperature gradient through liquid-vapor phase change process compared to a single phase heat transfer [1]. Due to such technical advantages, the nucleate boiling is widely used in refrigeration, thermoelectric power generation, and industrial processes [2–4]. However, the undesired vapor-liquid, two-phase flows near the boiling surface leads to limited Heat Transfer Coefficient (HTC) and poor Critical Heat Flux (CHF), which in turn results in inefficient system performance and catastrophic system burnout. To address these technical challenges, various engineered surfaces have been examined using subtractive and additive manufacturing techniques by providing a greater number of bubble nucleation sites and tailored two-phase flows near the boiling surface [5–9]. Nucleation sites can be generated by simply roughening the surface or by employing a microporous coating on the boiling surfaces [10].

Since the first enhanced surface manufactured by cold metalwork was developed in the late 1960s, various tubular enhanced surfaces were developed which can be categorized into two groups. The one is the structured surface with integral fintubes having reentrant grooves or tunnels, and the other is porous surface having a plain tube with porous metallic matrix bonded on it [11,12]. The first enhanced surface with a reentrant cavity was reported in 1972 [13], and the one of the first studies on enhanced surfaces was conducted by Nakayama and Nakajima [14]. They tested the boiling heat transfer of R-11 on the porous surfaces by varying the pore diameter and system pressure from 0.05 to 0.15 mm and 0.04 to 0.23 MPa, respectively. The enhanced surface with a pore diameter of 0.1 or 0.15 mm showed the best performance at the system pressure of 0.23 MPa which means the system pressure and pore diameter have an influence on the heat transfer. Webb and Pais [15] tested four enhanced tubes (GEWA K-26, GEWA TX-19, GEWA-SE, and Turbo-B) on five low and highpressure refrigerants (R-11, R-12, R-22, R-123, and R-134a) at saturation temperatures of 4.4 and 26.7°C. The high-pressure refrigerants (R-12, R-22, and R-134a) showed improved pool-boiling per-

<sup>\*</sup> Corresponding author.

E-mail address: gisuk,hwang@wichita.edu (G. Hwang).

#### **Nomenclature** С slope of the boiling curve $C_H$ Hamakar constant (J) growth period constant $C_{tg}$ specific heat (J/kg-K) $c_p$ $d_b$ departure bubble diameter (m) $d_p$ pore diameter (m) f bubble generation frequency (1/s) gravitational acceleration (m/s<sup>2</sup>) g h heat transfer coefficient (W/m<sup>2</sup>-K) heat of vaporization (J/kg) $\Delta h_{lg}$ thermal conductivity (W/m-K) k $l_p$ groove mouth spacing (m) $L_p$ pore center to center spacing (m) $N_A$ mean number density of active nucleation sites $(1/m^2)$ pressure $(N/m^2)$ or pitch (m)р heat flux (W/m<sup>2</sup>) q surface s Τ temperature (K) $\Delta T$ wall superheat (K) time (s) t W tunnel width (m) Greek symbols dynamic viscosity (N/m<sup>2</sup>-s) $\mu$ density (kg/m<sup>3</sup>) ρ surface tension (N/m) σ Subscripts bubble cric critical ex external experimental exp growth period g 1 liquid pore p pred prediction red reduced S substrate sat saturation tip tip tun tunnel vapor v waiting period w

formance compared to low-pressure refrigerants (R-11 and R-123) which was due to different thermophysical properties of the refrigerants, i.e., surface tension, latent heat of vaporization etc. Furthermore, a high HTC was observed at high saturation temperature compared to the HTC at low saturation temperature for all the tested enhanced surfaces. Chien and Webb [16] investigated the pool boiling with methanol on the finned copper surfaces having pores of 0.23 mm diameter and sub-surface tunnels. They observed the tunnel condition through the high-speed camera to find that at high heat flux, almost all the tunnel area was vapor-filled except the liquid menisci on the sharp corners. They concluded that the main heat transfer mechanism in the tunneled surfaces is mainly dictated by the sharp menisci in the corner. In continuation to the previous study, Chien and Webb [17] investigated the pool boiling of R-123 on the structured surfaces having pore diameters of 0.18 and 0.23 mm. They also reported the dynamic characteristics of bubbles such as bubble departure diameter, number of nucleation sites, and bubble generation frequency, and found that the enhanced surfaces increased the number of bubbles compared to the plain surface. The similar trend was observed for the nucleation sites as Kedzierski and Lin [18] investigated the pool boiling of R514A, R1224yd(Z), and R1336mzz(e) on the flat and turbo-ESP surfaces. As compared the results with the R-123, they found that the heat flux increased using R514A, R1224yd(Z), and R1336mzz(e) by 30%, 57%, and 13%, respectively. Detailed discussions about the boiling on enhanced surfaces can be found in the literature [19–25].

As for the predictive models on the pool boiling HTC on the enhanced surfaces, Nakayama et al. [26,27] developed a semiempirical model for the porous surfaces, for the first time based on their pool-boiling experimental data using N2, R-123, R-11, showing 80-90% enhancement compared to the plain surface. They developed the model based on the suction-evaporation model having seven empirical constants, assuming that the total heat flux in the porous surface is contributed by tunnel and external heat flux. Webb and Pais [15] tested four enhanced surfaces on five refrigerants and proposed a correlation using a power law to predict the HTC. Later on, through a series of experiments, Chien and Webb [28] proposed a dynamic model by including the temporal variation in evaporation through the tunnel, while modifying Nakayama model [27]. Their model includes only two empirical constants and external heat flux was predicted through the Haider and Webb Model [24]. Kim and Choi [29] performed pool boiling experiments on the three enhanced tubes having pore size of 0.20, 0.23, and 0.27 mm with connecting gaps at two saturation temperatures, 4.4 and 26.7°C. Similar to previous studies, they also noted that HTC was higher at high saturation temperature owing to favorable thermophysical properties, i.e., low surface tension and high heat of vaporization. They modified the Cooper correlation to incorporate the pore diameter effect to predict the data within the error band of  $\pm 20\%$ . Ramaswamy et al. [30] obtained the bubble growth data during the boiling of FC-72 on the silicon wafer having mini channels. They noted that diameter of the departing bubble increased with the increase in pore diameter and a greater number of pores got active with the increase in heat flux synergizing the previous findings that heat flux and pore diameter are one of the influential parameters and have an impact on the heat transfer performance. Based on bubble dynamics data, they developed a detailed model to predict bubble departure diameter, frequency, nucleation site density, and heat flux. Pastuszko et al. [11,31-36] carried out a series of pool boiling experiments using ethanol, water, FC-72, Novec-649 on enhanced surfaces and derived a static model to predict the bubble dynamics parameters and HTC. Their model predicts the HTC with the error band between  $\pm 30$  to  $\pm 40\%$ [11]. Recently, Kedzierski and Lin [37] developed a model for the flat turbo-ESP surface during the pool boiling of R1234ze(e), R515A, and R1233zd(e) which fitted into their experimental data reasonably.

However, the previous models did not reasonably predict the experimental results on different surface geometry or operational conditions, showing that the error can be as high as  $\pm 50\%$  [21,22]. The large error is related to the convoluted relations between the complex boiling process, various surface geometries, thermophysical properties, and operating conditions. Thus, it is imperative to seek an advanced model to accurately predict the pool boiling performance on various surfaces and operation conditions. Emerging Artificial Intelligence (AI)-based models offer to predict the pool boiling performance on enhanced surfaces with the desired accuracy by unlocking such convoluted relations [38–45], but it was not reasonably implemented into the boiling performance prediction on enhanced surfaces yet. In this study, we examine the complex relations among four geometrical, nine thermophysical properties, and two operational conditions to accurately predict the HTC on enhanced surfaces such as porous, sub-tunnels, reentrant cavity, or

**Table 1** Values for coefficient C and exponent n for Eq. (1).

Surface type	Refrigera	nt Satur	ration temperature, 4.4°C	Saturation	temperature, 26.7°C
GEWA K26	_	С	n	С	n
	R-11	2.30	0.726	44.16	0.470
	R-12	41.70	0.519	69.71	0.490
	R-22	59.72	0.509	56.71	0.529
	R-123	60.43	0.489	102.59	0.452
	R-134a	2.87	0.706	47.34	0.472
GEWA TX19	R-11	1.50	0.779	8.53	0.646
	R-12	155.79	0.394	78.79	0.476
	R-22	191.11	0.389	133.07	0.451
	R-123	105.05	0.423	126.02	0.417
	R-134a	2.35	0.731	12.65	0.591
GEWA SE	R-11	2.47	0.739	4.92	0.733
	R-12	189.85	0.421	633.58	0.327
	R-22	346.88	0.380	392.21	0.385
	R-123	172.78	0.421	100.97	0.487
	R-134a	1.57	0.776	2.85	0.764
Turbo-B	R-11	830.46	0.298	1531.97	0.249
	R-12	205.98	0.429	646.49	0.326
	R-22	296.57	0.397	200.47	0.452
	R-123	304.44	0.389	1455.51	0.240
	R-134a	170.21	0.402	274.72	0.361

fin geometries over a flat plate and tube surfaces, while those parameters are incorporated into six dimensionless numbers as input parameters. The obtained predictions are also compared with the predictions using the existing empirical model to show the accuracy improvement.

#### 2. Methodology

#### 2.1. Existing models

Although there are several existing empirical/semi-empirical models for pool boiling HTC on the enhanced surfaces in the literature [11,15,24,27-29,31,36,37,46-48], only three kinds of models are selected as a reference. The first one [15] is a conventional correlation similar to power law developed on the database of five refrigerants and four enhanced tubes at two operating temperatures, second one [29] is an extended form of Cooper correlation[49] developed for the pool boiling of three enhanced tubes on three refrigerants operating at two saturation temperatures. The last model [36] is a detailed bubble dynamics based model developed on the database of pool boiling of FC-72 and water on micro-finned surfaces.

#### 2.1.1. Webb and Pais model

Webb and Pais [15] developed an empirical model based on the measured HTC, h, using the pool boiling with five refrigerants (R-11, R-12, R-22, R-123, and R-134a) on four boiling tubes having enhanced surfaces (GEWA K-26, GEWA TX-19, GEWA-SE, and Turbo-B) at saturation temperature of 26.7 and 4.4°C as given as

$$h = Cq^n \tag{1}$$

where C and n are fitting parameters for different refrigerants, operational conditions, and types of enhanced surfaces. The values of coefficients C and n recommended by the authors are listed below in Table 1, and the schematics of the enhanced surface structures are shown in Fig. 1.

#### 2.1.2. Kim and Choi model

Kim and Choi [29] tested three refrigerants on enhanced surfaces having pores with connecting gaps. Similar to Cooper correlation [49] for the plain surfaces, they correlated the HTC with system pressure and surface geometry. For R-11 and R-123, we have

$$h = 112.2q^{0.523}p_{red}^{0.254}(-1.13 - 97600d_p + 9.40 \times 10^8d_p^2 - 2 \times 10^{12}d_p^3)$$
(2)

and for R-134a, we have

$$h = 10^{11} q^{0.297} p_{red}^{0.632} d_p^{2.1} (3)$$

where q is the heat flux,  $p_{red}$  is the reduced pressure and  $d_p$  is the pore diameter.

#### 2.1.3. Pastsuzko and Wojcik model

Recently, Pastsuzko and Wójcik [36] developed a semianalytical model by analyzing the measured bubble dynamics in the pool boiling using water and FC-72 on micro-finned surfaces with and without perforated foil at atmospheric pressure. In Pastsuzko and Wojcik model, the HTC is calculated as

$$HTC = \frac{q}{\Delta T} \tag{4}$$

where q is total heat flux and  $\Delta T$  is the wall superheat.

The total heat flux is obtained from

$$q = q_{tun} + q_{ex} \tag{5}$$

The evaporation heat flux in the tunnels,  $q_{tun}$ , was calculated as

$$q_{tun} = \rho_{\nu} \Delta h_{lg} N_A \frac{\pi d_b^3}{6} f \tag{6}$$

where the  $\rho_{v}$  is the vapor density,  $\Delta h_{lg}$  is the heat of vaporization,  $N_{A}$  is the mean density of nucleation sites, given as

$$N_{A} = \frac{4W_{tun}}{\pi d_{b}^{2}} \frac{1}{P_{tun}} \tag{7}$$

where the  $P_{tun}$  is the spacing between sub-tunnels, and the  $W_{tun}$  is the width of the tunnel. Here, the  $4W_{tun}/\pi\,d_b^{\ 2}$  denotes the number of active pores per tunnel, which is obtained by dividing the tunnel width by the cross-sectional area of the departing bubble. The bubble departure diameter of the departing bubble,  $d_b$ , and frequency, f, of the bubble are obtained from

$$d_b = \left[\frac{6\sigma d_p}{g(\rho_l - \rho_v)}\right]^{1/3} \tag{8}$$

$$f = \frac{1}{t_w + t_\sigma} \tag{9}$$

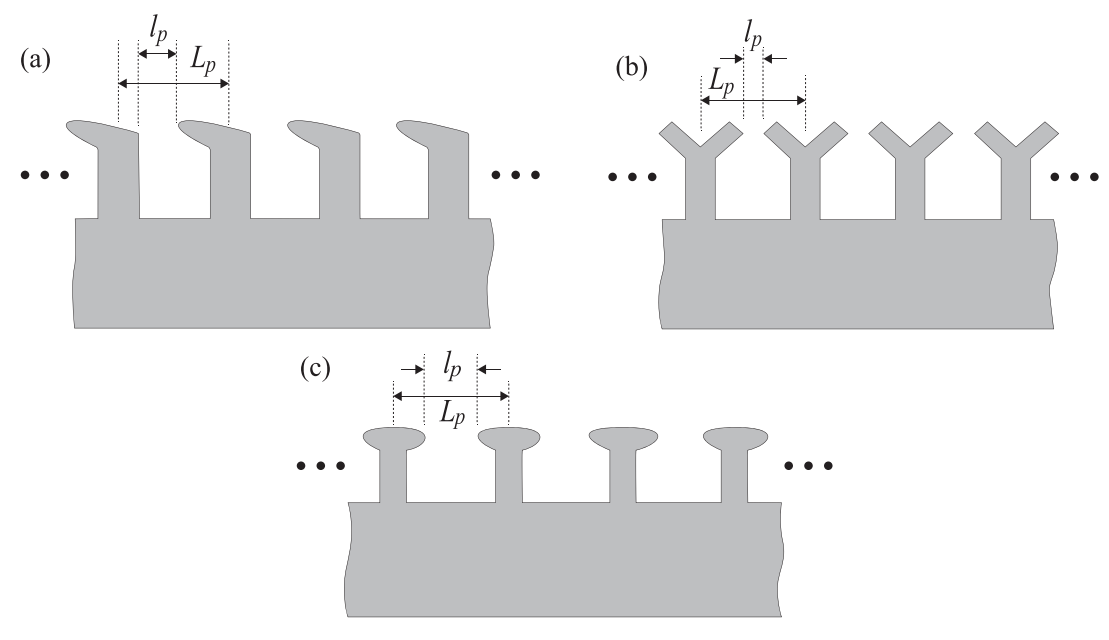


Fig. 1. Schematic of enhanced surfaces tested by Webb and Pais [15], (a) Turbo-B, (b) GEWA SE, and (c) GEWA TX19.

**Table 2**Summary of the input parameters including range, mean, and standard deviation.

Parameters	Range	Mean (µ)	Standard deviation $(\sigma)$
Liquid thermal conductivity	$0.057 \le k_l \le 0.67 \text{ W/m-K}$	0.14 W/m-K	0.179 W/m-K
Latent heat of vaporization	$138 \leq \Delta h_{lg} \leq 2256 \text{ kJ/kg}$	378 kJ/kg	629 kJ/kg
Pore diameter/fin spacing at the tip	$0.05 \le l_p \le 1.03 \text{ mm}$	0.24 mm	0.17 mm
Specific heat capacity	$640.7 \le c_p \le 4215 \text{ J/kg-K}$	1,356 J/kg-K	982 J/kg-K
Absolute pressure	$0.039 \le p \le 1.09 \text{ MPa}$	0.28 MPa	0.295 MPa
Surface tension	$7.87 \le \sigma_l \le 58.9 \text{ mN/m}$	17.9 mN/m	14.3 mN/m
Wall superheat	$0.39 \leq \Delta T \leq 109.6 \text{ K}$	6.29 K	10.95 K
Pore/fin pitch	$0.25 \leq L_p \leq 3 \text{ mm}$	1.2 mm	0.86 mm
Temperature	$4.4 \le T \le 100  ^{\circ}\text{C}$	28 °C	28.3 °C
Heat flux	$1.95 \le q \le 602 \text{ kW/m}^2$	49 kW/m <sup>2</sup>	91.39 kW/m <sup>2</sup>

where,

$$t_{\rm W} = 3\Delta t_{\rm g} \tag{10}$$

and

$$t_g = \frac{1}{0.0296} \left[ \frac{7}{\pi} \frac{\rho_l T_{sat}}{i_{lv} \rho_v \Delta T} \frac{(d_b + d_p)}{(d_b - d_p)} \right]^{1/2} \left( \frac{d_b - d_p}{2} \right)$$
(11)

The external heat flux,  $q_{ex}$ , is obtained from Mikic and Rohsenow [50] correlation, given as

$$q_{ex} = 2\sqrt{\pi k_l \rho_l c_{pl} f} d_b^2 N_A \Delta T_{tip}$$
(12)

#### 2.2. Data collection

To check the accuracy of the existing empirical models, i.e., Eqs. (1)–(3), and train and validate the model, the experimental data are extracted from previous studies [15,22,29,36,51]. The working fluids are R-11, R-12, R-123, R-134a, R-22, FC-72 and water, and the enhanced tubes include GEWA K-26, GEWA TX-19, GEWA-SE, Turbo-B, tubes having pores with connecting gaps, porous surfaces having rectangular tunnels and micro-fins with and without sintered perforated foil. The total 1256 experimental data points were used to develop the model and to predict the HTC. The key thermophysical parameters and operation conditions are given in Table 2, and the working fluids and the numbers of data points are provided in Table 3.

#### 2.3. Deep neural network model

Artificial neural networks (ANNs) are widely used machine learning methods to unlock the complex relations in large multidimensional datasets. With the help of advance libraries, they offer predictive tools to reasonably identify the underlying functional relationship among the data for desired accuracy without physicsbased complex equations. There are various types of neural network models available, and their usage depends on the types of the data. For example, the Recurrent Neural Network (RNN) is implemented by Jiang et al. [52] to predict the surface temperature of the Li-ion battery at ambient conditions, Nie et al. [53] developed a Convoluted Neural Network (CNN) based model to recognize the flow pattern though two-phase flow images. A neural network with more than one hidden layer is usually referred as a deep neural network (DNN) [54]. Deep neural networks are suitable for regression problems and have been used for various thermal problems as well. More details can be found in the literature [39,40,45,55]. In this study, the DNN is developed and used to predict the heat transfer coefficient due to the regressive nature of the problem as the detailed approach is given below. The DNN is composed of three layers of nodes: an input layer, an output layer, and an arbitrary number of dense/hidden layers, placed in between the inputs and outputs, each with a pre-defined number of neurons. In the neural network, a number of activation functions can be used, but in this study, Rectified Linear Unit (ReLU) was implemented in each layer except the output layer [56]. The selection of the type of

**Table 3**Pool boiling data on enhanced surfaces including working fluid and number of data points.

Previous work	Working fluid	Number of data points
Webb and Pais [15]	R-11, R-12, R-22, R-123, R-134a	313
Kim and Choi [29]	R-11, R-123, R-134a	221
Pastuszko and Wojcik [36]	Water, FC-72	122
Mondal and Kim [22]	R-134a	288
Mehdi and Kim [51]	R-123	312

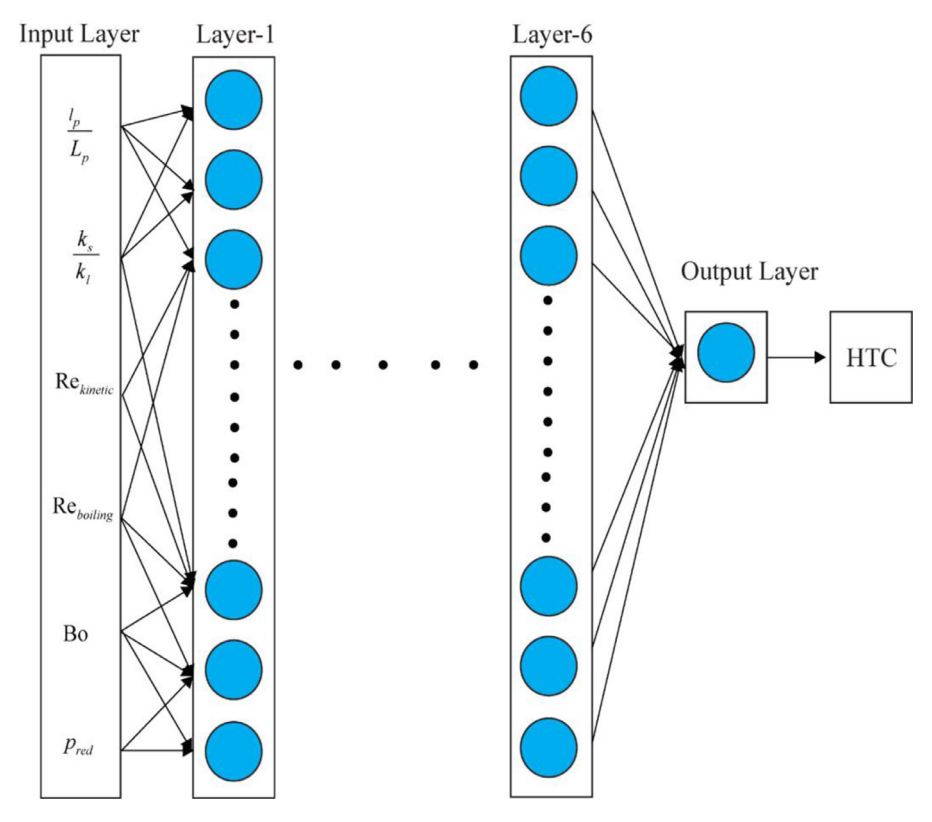


Fig. 2. Schematic of DNN model including the input/dense/output layers, and input and output parameters.

the activation function mainly depends on the problem to be addressed and the user choice. In this study, as only one prediction of HTC is needed, so "linear function" was implemented in the output layer. The structure of the neural network used in this study is shown in Fig. 2. The key input parameters as dimensionless numbers and the output parameter, HTC, are also shown. The model was developed in Python (Version 3.8.8) [57] with Scikitlearn [58], Keras [59], Matplotlib [60], Pandas [61], and Seaborn [62] libraries and it was trained by varying:

- i Number of dense layers from 2 to 8 and number of neurons from 30 to 512.
- ii Number of epochs between 100 and 20,000.
- iii Optimizers and learning rate.
- iv Batch size (10, 32, and 64).

The detailed parameters of the optimized DNN model are listed in Table 4.

#### 2.3.1. Selection of input parameters

The input parameters are selected based on the literature survey and empirical correlations reported in literature [6,14,15,21,22,24,25,27–29,35,36,51,63–66]. The nucleate boiling heat transfer performance strongly depends on the structural, material, and operational properties, and the six dimensionless parameters are identified by combining the properties.

As shown in Fig. 2, the first input parameter is the ratio of the pore diameter or fin spacing at the tip to the pore or center to center fin spacing,  $l_p/L_p$ , which represents the characteristic boiling surface geometries. This parameter is a critical geometrical dimensionless number since the pore diameter or groove mouth spacing and pore or fin pitch control the HTC of the enhanced surfaces [22,29,64]. The smaller pore or groove mouth spacing increases the nucleation site density, and capillary pressure, while the larger pore or groove mouth spacing increases the permeability which is required at high heat fluxes to increase liquid supply, and it also increases departure bubble diameter. Similarly, the smaller pore or fin spacing decreases the bubble departure diameter and increases the nucleation sites, while the larger pore or fin spacing reduces the nucleate site density. The typical range of the  $l_p$  and  $L_p$  are 0.98 and 2.75 mm in the current DNN model.

The second input parameter is the ratio of the thermal conductivity of the boiling surface to the thermal conductivity of the liquid, i.e.,  $k_s/k_l$ . The larger the thermal conductivity of the liquid, the larger heat transfer occurs by the departing bubbles and vice-versa. Similarly, the large thermally-conducting surface helps quickly evaporate the liquid, and in turn increase active nucleate site density [66]. The values of  $k_l$  are between 0.057 and 0.67 W/m-K, while only one value of  $k_s = 401$  W/m-K is used because the selected boiling surfaces are copper.

**Table 4** Summary of model parameters.

Parameter Value		Parameter	Value
No. of dense layers (No. of neurons per layer)	6 (50-100-150-300-250-150)	Random state	None
No. of inputs	6	Regularization	L2
No of outputs	1	Batch size	64
Learning rate	0.001	Optimizer	Adam
Activation	ReLU	Drop out	0.01
Scalar	Standard scalar	Epochs	15,000

The third parameter is the kinetic Reynold number to include the effects of the wall superheat,  $\Delta T$ , along with the specific heat of liquid  $c_{p,l}$  and the heat of vaporization  $\Delta h_{lg}$ , which is essential to HTC [see, Eq. (4)], given as

$$Re_{kinetic} = \frac{c_{p,l}\Delta T}{\Delta h_{lg}}.$$
 (13)

The fourth parameter is the boiling Reynold number which incorporates the heat flux along with the pore diameter/ groove mouth spacing at the tip  $l_p$ , dynamic viscosity  $\mu_l$ , and heat of vaporization,  $\Delta h_{lg}$  in the dimensionless form, given as

$$Re_{\text{boiling}} = \frac{ql_p}{\mu_l \Delta h_{lg}}.$$
 (14)

To include the effects of the bubble dynamics as a result of the force balance between the surface tension,  $\sigma$ , and gravity (or bouncy force), the bond number, Bo is used as the fifth parameter, given as

$$Bo = \frac{\Delta \rho_{lg} g l_p^2}{\sigma} \,. \tag{15}$$

where  $\Delta \rho_{lg}$  is the density different between the vapor and liquid, g is the gravitational acceleration,  $l_p$  is the pore diameter or the groove mouth spacing. Surface tension has a significant impact on the size of the generated bubble as reported in various studies [27,28,66]. For instance, in Pastuszko and Wojcik model Eq. (8), the departure diameter was found to be proportional to cube root of surface tension.

Moreover, as reported in literature [14,29,49,67], the larger system pressure results in the higher heat transfer mainly due to the favorable thermophysical properties, e.g., the larger vapor density at the elevated pressure, and the reduced pressure,  $p_{red}$ , the ratio between the operational and critical pressure is considered as the sixth parameter, given as

$$p_{red} = \frac{p}{p_{cric}} \,, \tag{16}$$

where the p is the system pressure, and  $p_{cric}$  is the critical pressure.

Furthermore, a correlation matrix, so called heat map, was generated by using the pandas Spearman's correlation method [68], as shown in Fig. 3. The association of HTC with the input parameters can be seen from the correlation coefficient values in the last row of the correlation matrix. As shown in Fig. 3, we can see that all the selected parameters have an impact on the experimental heat transfer coefficient, HTC.

The graphical relations among the six input parameters, i.e., geometrical, thermophysical, and operational dimensionless numbers, and one output parameter, HTC, are shown in Fig. 4. It shows that the highest HTC was obtained from water and R-134a due to superior thermophysical properties and lowest values of HTC were observed from FC-72 due to highly wetting nature and other poor thermophysical properties. Moreover, the large range of the scatter among the parameters in the dataset is identified, and this in

turn becomes challenging to predict the HTC using simple empirical correlations. In this study, this challenge is addressed using the developed DNN.

#### 2.3.2. Model training

An accurate neural network model requires reasonable data type and numbers. The most influential parameters were used in a dimensionless form to develop the model. In this study, the total of 1256 data points were used. The 60–90% of the data were used to train the neural network model and validate the model, while the remaining 10–40% of the data were used to test the model. As the input parameters have different scale so to reduce the bias, the data was normalized by using Scikit learn Standard Scalar function [69], and later, the predictions were transformed to original scale. Furthermore, the random dropping was also implemented to improve the model accuracy [70]. The model accuracy was measured using the Mean Absolute Percentage Error (MAPE) and the optimization was performed by Adam optimizer [71], and the Keras library [72] was used to develop the DNN. The MAPE is given as

MAPE = 
$$\frac{1}{n} \sum_{i=1}^{n} \left| \frac{h_{\text{exp}} - h_{pred}}{h_{\text{exp}}} \right| \times 100 \ (\%)$$

where n is the total number of data points,  $h_{exp}$  is the experimental HTC,  $h_{pred}$  is the predicted HTC. The best performing model was saved, and the HTC was predicted using test data. The model loss was calculated for validation, and the predicted MAPEs both for the training and validation with respect to the numbers of epochs for the train-test ratio of 90/10% are shown in Fig. 5. The predicted MAPE exponentially decreases as the numbers of epochs increase, and the MAPE reaches below 5% at 5000 epochs. The fluctuations of MAPE were related to the use of a stochastic gradient descent (SGD) approach. The predictability of the DNN model depends on the nature of the data and the amount of training data. Initially, each dataset was trained and tested separately five times with randomly selected data to ensure the prediction repeatability and estimate the variations. The predicted mean MAPE is reported with the error bar. For each training/testing, the different dataset was randomly selected to avoid the duplicate prediction.

#### 3. Results and discussion

#### 3.1. HTC prediction using existing models

To examine the accuracy of the existing empirical model [15,29,36], we calculate the error between the measured and predicted HTC as shown in Fig. 6. In Fig. 6(a), Eq. (1) predicts the experimental HTC with the maximum error of  $\pm 20\%$ . This empirical correlation predicts reasonably the experimental results compared to other alternatives, e.g., Fig. 6(b) and (c). However, this correlation requires numerous empirical coefficients, i.e., 80 combinations of the empirical coefficient C and exponent C and exponent C and exponent C and exponent of the empirical coefficient (see Table 1). Thus, it is challenging to predict other geometries, operational conditions, and working fluids where the fitting parameters are not available. Fig. 6(b) shows

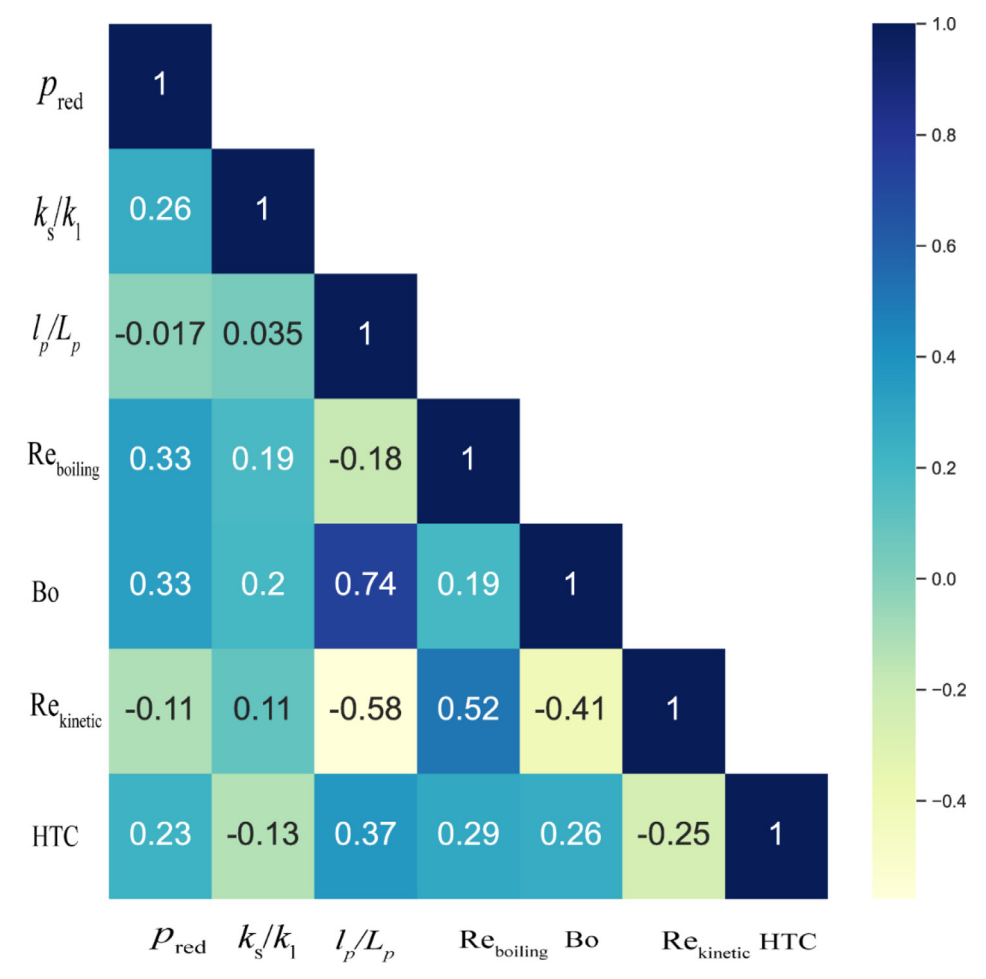


Fig. 3. Correlation matrix heat map between six input parameters (six dimensionless numbers) and one output parameter, HTC.

the comparison between the predicted HTC using the Pastuszko and Wojcik model and their experimental data [36]. The model predicts the 75% and 60% of the experimental data with water and FC-72 within  $\pm 35\%$  and  $\pm 40\%$ , respectively. The model overpredicts the experimental HTC at the low ( $h_{exp} = 300 - 1000 \text{ W/m}^2\text{-K}$ ) and high ( $h_{exp} \sim 10,000 \text{ W/m}^2\text{-K}$ ) heat fluxes. At low heat flux, this mainly results from the fact that the model overpredicts the numbers of nucleation sites compared to the realistic numbers of nucleation poor, i.e., flooded phenomena. Furthermore, at high heat flux, this model overpredicts the contribution of the nucleate boiling phenomena at small pores < 1 mm compared to the experimental observations, i.e., surface dryout phenomena. Fig. 6(c) shows the comparison between the predicted and measured HTC using Eqs. (2) and (3) and the experimental data from the same research group [29]. These equations predict 81% of the measured HTC (characteristic pore size of 0.2, 0.23, and 0.27 mm) within  $\pm 20\%$ .

In fact, these equations are a modified model based on the Cooper correlation (plain surface) [49], by adding the characteristic pore size of the enhanced surfaces. To further understand the predictability of the model, the comparison between the predicted HTC and similar experimental data from the same research group as shown in Fig. 6(d). Note that there are small pore size variations, i.e.,  $\pm 0.1$  mm pore size difference between the experiments with the characteristic pore sizes of 0.1, 0.2, and 0.3 mm. However, the model does not predict the similar experimental data, showing that only 48% of the experimental data can be predicted within

 $\pm 50\%$  error. The large error indicates that the existing model uses the oversimplified treatment of the complex nucleate boiling phenomena by using one geometrical parameter, i.e., pore size, Eq. (3).

Fig. 7 shows the comparison between measured HTC of Mehdi and Kim [51] and Mondal and Kim [22] and predicted HTC by the dynamic models of Chien and Webb [28] and Nakayama et al. [27]. As shown in Fig. 7(a), Chien and Webb [28] model significantly overpredicts the data with MAPE of 3557%, and it does not predict the HTC of the enhanced surfaces having  $L_p = 3.0$  mm. The excessive overprediction is related to a few reasons. Firstly, the enhanced surfaces have different geometries, i.e., tubular geometry for Chien and Webb [28], whereas horizontal plate for Mondal and Kim [22] and Mehdi and Kim [51], which potentially change the bubble dynamics near the enhanced surfaces. Secondly, this model uses two critical empirical constants based on their original experimental work, which may not reasonably predict the other experimental data. The first constant is a bubble growth constant,  $C_{tg} = 0.0296$ , which has a significant impact on the bubble generation frequency, and nucleation site density, which are crucial to HTC. The second is a Hamaker constant  $C_H = 2 \times 10^{-12} \text{J}$ , an inter-molecular interaction parameter, which in turn is critical to evaporation rate. A shown in Fig. 7(b), Nakayama model also significantly overpredicts the data with MAPE of 7019%. The substantial overpredictions are related to the fact that they use six empirical constants from the best-fit of their experimental data and the model was developed on the enhanced surfaces having pore pitch,  $L_p$ , between 0.6 and 0.72 mm, which are much smaller than

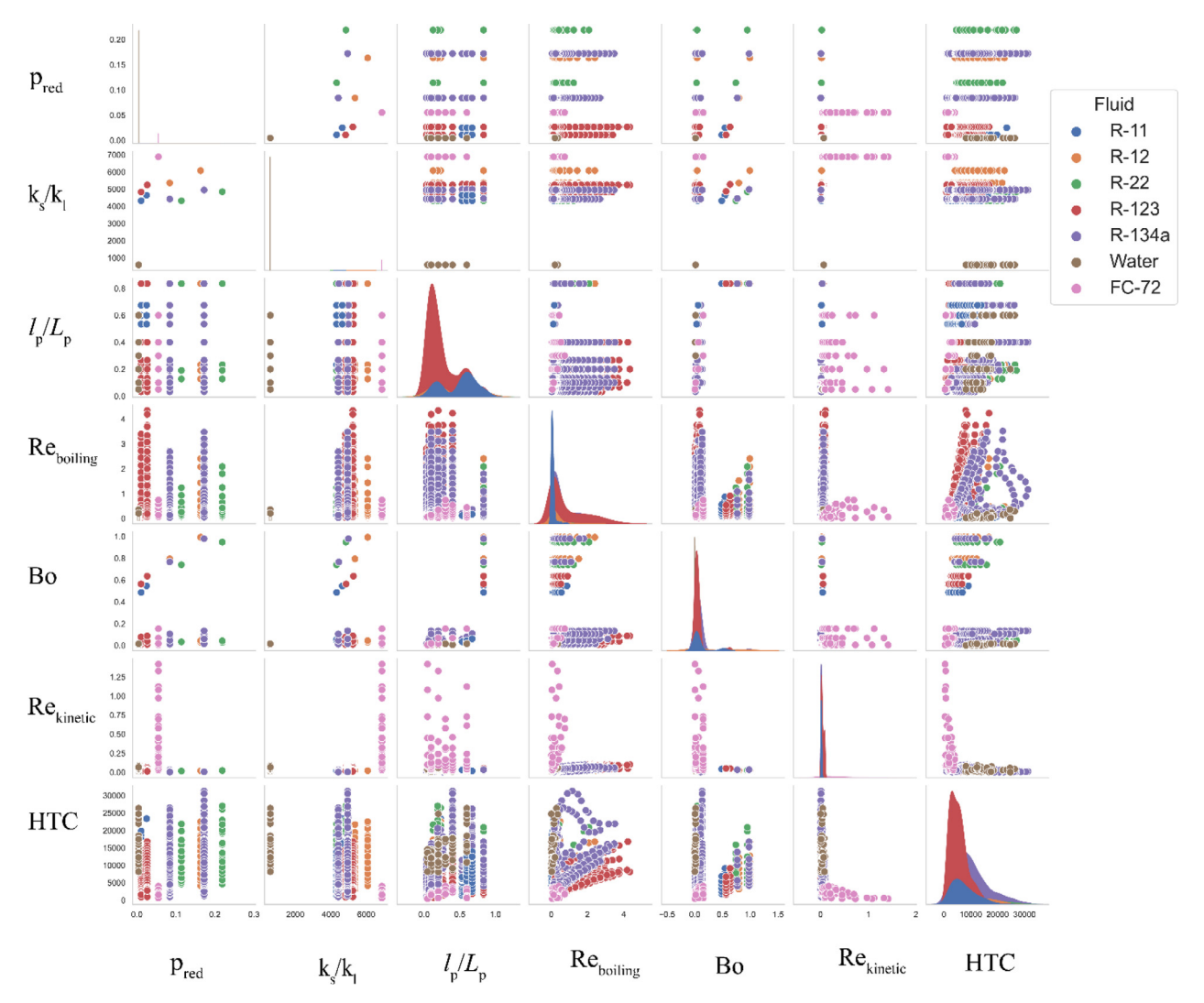


Fig. 4. Complex relations among the six input and one output parameters, i.e., HTC.

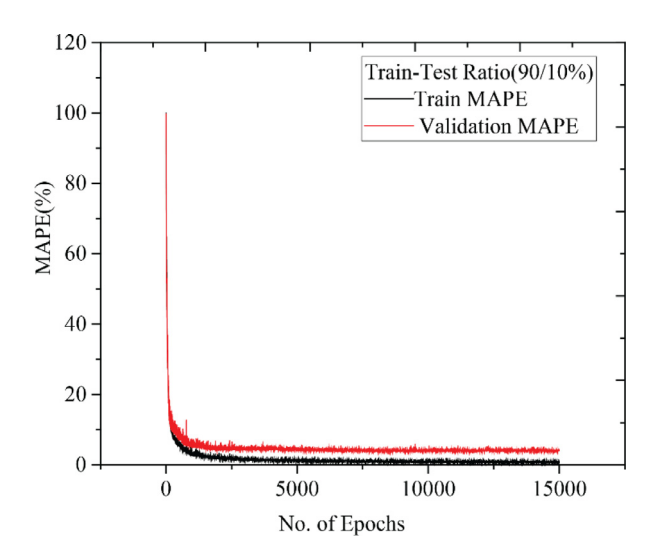


Fig. 5. Variations of MAPE of training and validation dataset with respect to the numbers of epochs for the final DNN model. The train-test ratio of 90/10% is shown.

 $L_p = 0.75$ , 1.5, and 3.0 mm in the experimental studies by Mehdi and Kim [51] and Mondal and Kim [22]. This indicates that the

pore pitch (or pore density) has a significant impact on the heat transfer performance, and the existing dynmic models cannot be extended to other experimental conditions. Details about the models can be found in the previous studies [26–28,64,73].

#### 3.2. Effects of train-test ratio on model accuracy

To investigate the effects of train-test ratio and the nature of the dataset on the model accuracy, we calculate the variation of MAPE with respect to the train-test ratio on various datasets [15,22,29,36,51] as shown in Fig. 8.

Note that the mean MAPE is reported with error bars, showing the maximum difference from the mean value obtained using 5 different test runs for given train-test ratio. Fig. 8(a) shows the MAPE of the DNN model for three datasets (Webb and Pais [15], Kim and Choi [29], and Pastsuzko and Wojcik data [36]) as a function of the training ratio from 60 to 90%, and the MAPE monotonically decreases as the train-test ratio increases. Note that for the prediction of Webb and Pais [15] data, the GEWA K26 case was excluded due to the lack of the detailed geometrical information. This reduction is related to the fact that the DNN model improves the prediction accuracy as more data are used for DNN training. Fig. 8(a) also shows that the maximum MAPE of the Webb and Pais [15] and Kim and Choi [29] datasets is only 12.87%, whereas the MAPE of Pastsuzko and Wojcik data [36] is much larger. This

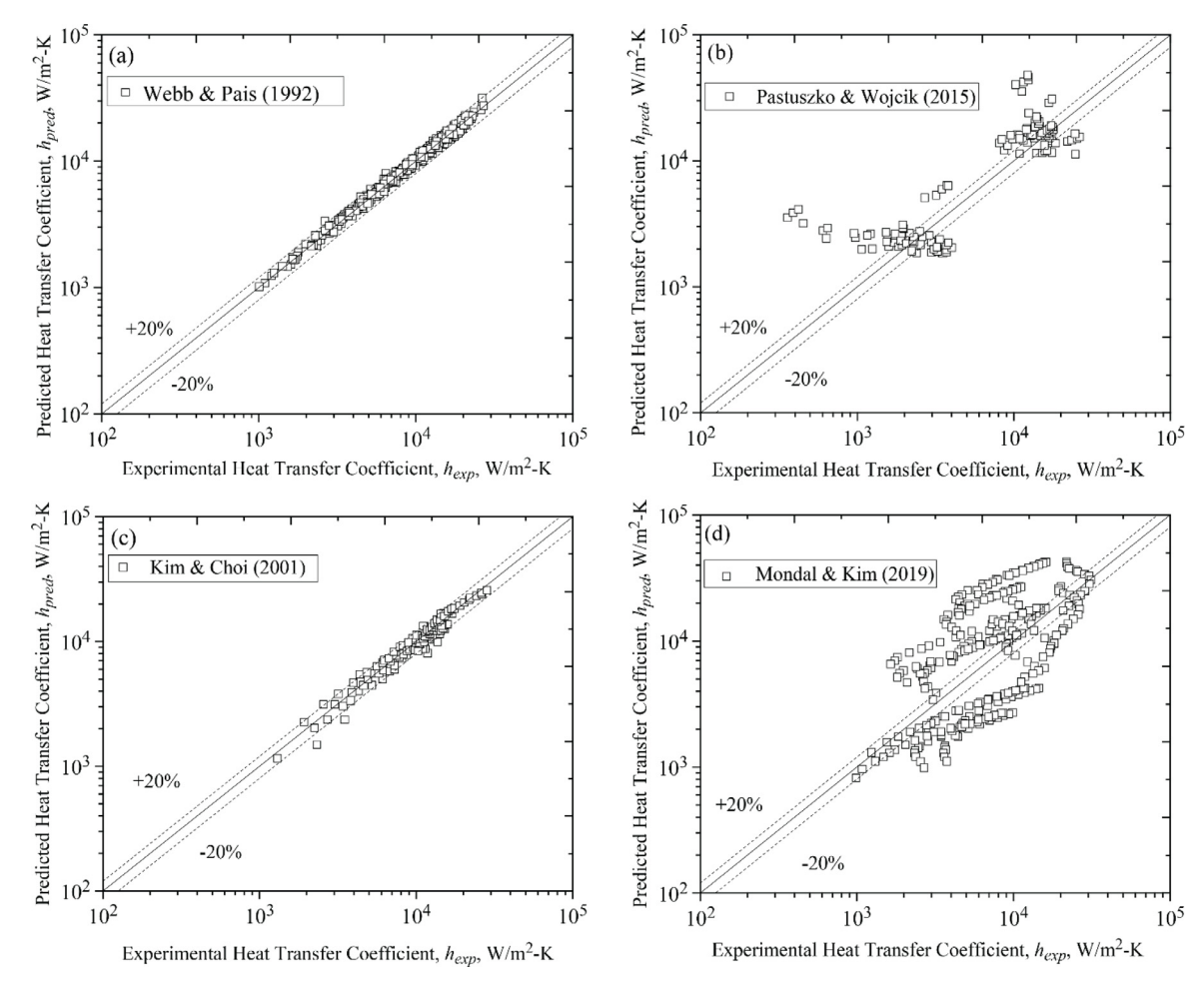


Fig. 6. Predicted HTC by empirical correlations (a) Webb and Pais [15], (b) Kim and Choi [29], (c) Pastsuzko and Wojcik [36] and (d) Mondal and Kim [22] predicted by Kim and Choi correlation [29].

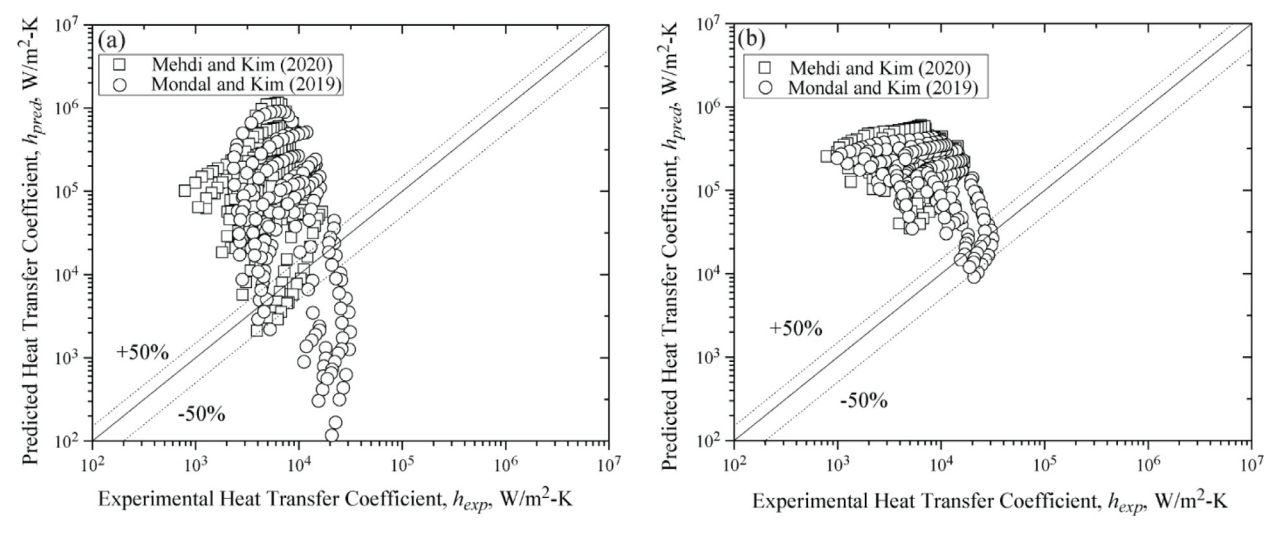


Fig. 7. Predicted HTC of the experimental pool boiling HTC by Mehdi and Kim [51] and Mondal and Kim [22] using dynamic models by (a) Chien and Webb [28], and (b) Nakayama et al. [27].

larger MAPE is related to the two reasons. Firstly, the experimental work by Pastsuzko and Wojcik [36] uses two different working fluids (water and FC-72), i.e., significantly different thermophysical properties, and this in turn results in large variations of the experimental HTC, i.e., large error bars. Secondly, the experimental data have only 122 data points. The significant variation in thermophys-

ical properties and corresponding HTC values within just 122 data points is not ideal to train the DNN, which in turn results in poor model accuracy. However, note that the MAPE drastically reduces as the train-test ratio increases. To identify the prediction accuracy improvement of the DNN model compared to existing models, the MAPE of DNN model for each experimental dataset is compared

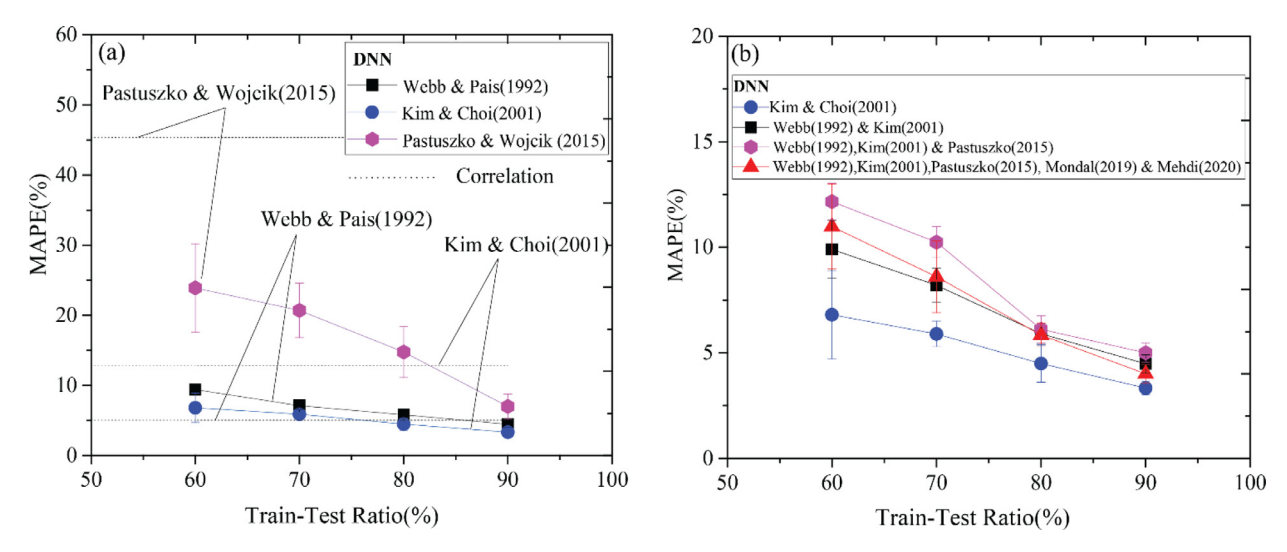


Fig. 8. Effects of the test-train ratio on the MAPE of (a) Webb and Pais [15], Kim and Choi [29], Pastsuzko and Wojcik [36] datasets including the predictions using the existing models, i.e., Eqs. (1)–(3) and Pastsuzko and Wojcik model, (b) the cumulatively combined datasets. Error bars are also shown.

to their own empirical/semi-empirical models. The DNN model for the Pastsuzko [36] and Kim and Choi [29] dataset outperforms the existing models for all the train-test ratio, while it shows the smaller MAPE for Webb and Pais [15] dataset only at 90–10 traintest ratio. Note that the correlation uses the specific surfaces at given operational conditions, which in turn results in predicting the experimental data reasonably as discussed in Section 3.1.

To investigate the effects of different experimental results on the DNN model accuracy, the different combinations of the datasets are used for the DNN training and testing. The predicted MAPE as a function of train-test ratio is shown in Fig. 8(b). The smallest MAPE is predicted using the data from Kim and Choi [29] which could be due to the minimal variations in the geometry (i.e., pore diameter was varied from 0.2 to 0.27 mm and pore pitch was varied from 0.37 to 0.4 mm). So, the data of remaining references [15,22,36,51] was added gradually to the model. The MAPE increases primarily due to the data scatter from the different thermophysical properties of the working fluids and surface geometries. For instance, the data of Webb and Pais [15] additionally add the pool boiling HTC using R-12 and R-22 to the Kim and Choi [29] dataset. Also, the fin pitch/fin gap size,  $L_p$ , is larger, i.e., 0.6, 0.94, and 1.33 mm, for the Webb and Pais [15] than those tubes, i.e., 0.374, 0.384, and 0.4 mm, tested by Kim and Choi [29]. Additional increase in MAPE is observed by adding the Pastsuzko and Wojcik datasets [36], similar to the increased MAPE by adding Webb and Pais [15] to Kim and Choi [29] datasets. However, the MAPE reduces by adding Mondal and Kim [22] and Mehdi and Kim [51] datasets to the previous two datasets. This reduction is related to the fact that the dataset [22,51] has 600 data points, which were obtained on the working fluids having similar thermophysical properties to the existing data. In other words, the DNN model accuracy increases as the numbers of the similar data increase. Similar to Fig. 8(a), the MAPE also decreases as train-test ratio increases for all the datasets, and the data heterogeneity effects are minimal at train-test ratio of 90/10%.

### 3.3. HTC Predicted by deep neural network

To identify the validity of the DNN model accuracy, we use the randomly selected 10% of all the pool boiling experimental data (126 data points, see Table 3) to compare with the DNN predicted HTC as shown in Fig. 9. The DNN model predicts the 93% of the experimental data within  $\pm 10\%$ , which outperforms one of the state-of-the arts existing correlation, i.e., Eq. (1). Note that it is challeng-

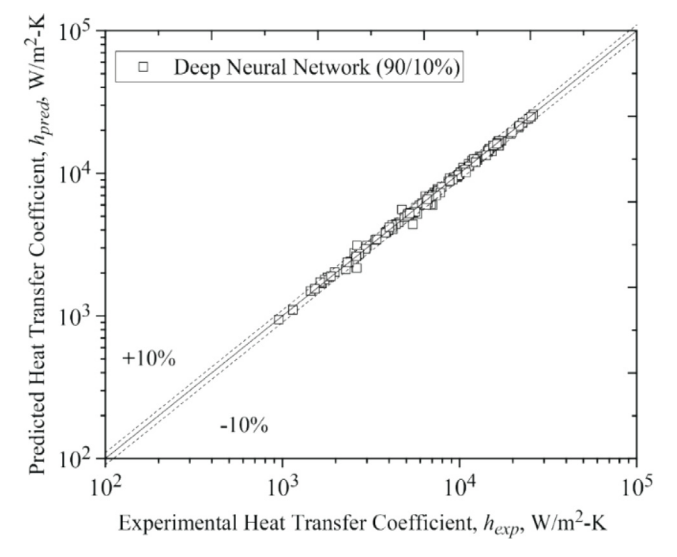


**Fig. 9.** Predicted HTC using DNN on the randomly selected 10% of the available experimental data (126 data points, Table 3) [15,22,29,36,51]. The  $\pm$  10% error bounds are also shown.

ing to compare the DNN model with Eq. (1), due to the lack of the empirical coefficients, C and n in Eq. (1) for the different experimental conditions. However, Eq. (1) predicts only 90% of their own experimental data within  $\pm 10\%$ .

To further validate the developed DNN model, the pre-trained model was used to predict the previous experimental pool boiling studies [34,74–76]. The predicted HTC vs the experimental HTC measured by Li et al. [76] are shown in Fig. 10(a). The current pre-trained DNN model predicts 84% of the data within  $\pm 30\%$  error bounds or 20% MAPE, which much improves compared to the existing empirical/semi-empirical models. For instance, Pastuszko and Wojcik model [36] predicts the Li et al. [76] data with only 40% of the data within  $\pm$  30% or 38% MAPE as shown in Fig. 10(b). Note that their study uses R141b and copper foam having circular channels, which are not used for the current DNN model training.

Fig. 11 compares the HTC predictions of the pre-trained DNN model with the experimentally measured HTC [34,74 75]. Fig. 11(a) shows the predictions of experimental data by Kumar and Wang [74] using the pre-trained DNN model. They measured the pool boiling HTC on the enhanced surfaces at three saturation temper-

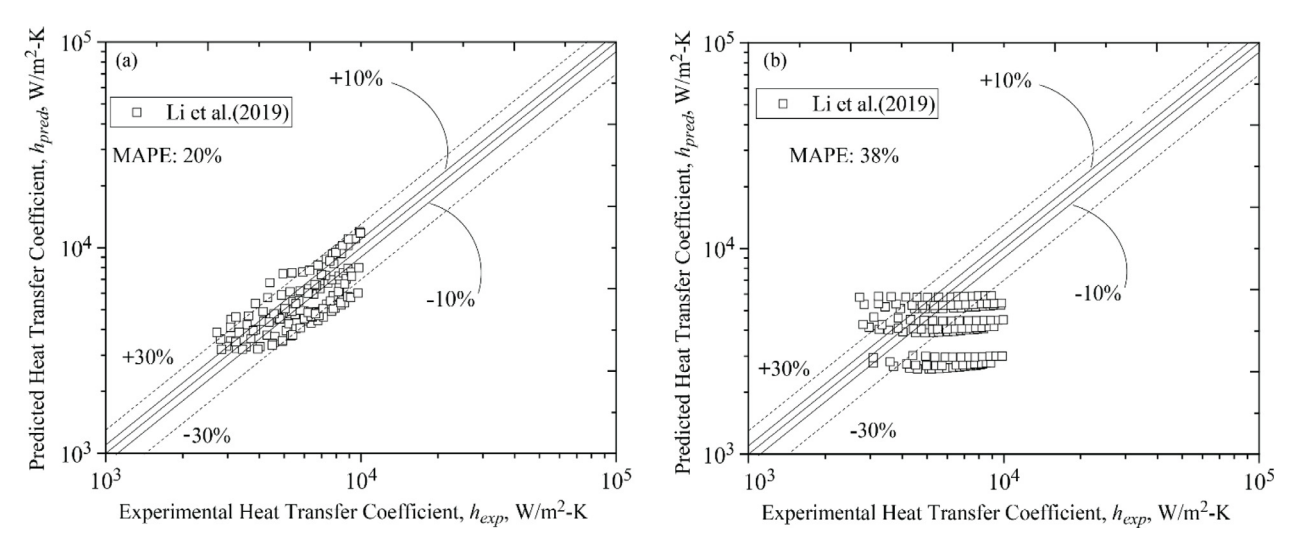


Fig. 10. Predicted HTC of Li et al. data [76] using (a) pre-trained DNN, and (b) Pastuszko and Wojcik model [36]. The MAPE and  $\pm$  10 and  $\pm$  30% error bounds are also shown.

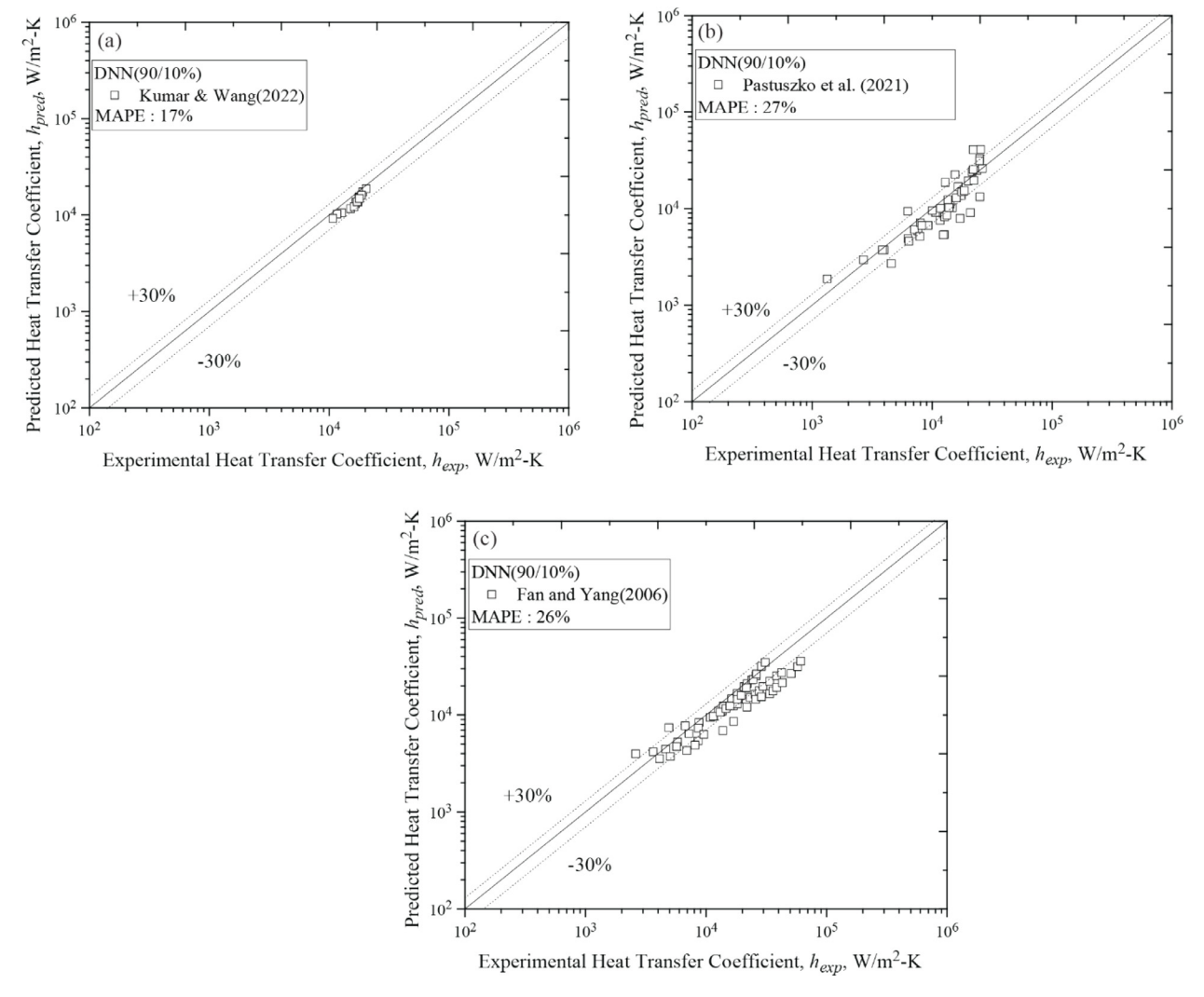


Fig. 11. Predicted HTC of (a) Kumar and Wang [74], (b) Pastuszko et al. [34], and (c) Yang and Fan [75] using pre-trained DNN.

**Table 5**Unseen data of enhanced surfaces including working fluid and number of data points.

Previous work	Working fluid	Number of data points
Tong Li et al. [76]	R-141b	135
Kumar and Wang [74]	R1234Ze(E)	15
Pastuszko et al. [34]	Novec-649	46
Yang and Fan [75]	R404A	60

**Table 6**Summary of the input parameters including range, mean, and standard deviation of chosen data.

Parameters	Range	Mean (µ)	Standard deviation $(\sigma)$
Pore diameter/groove mouth	$0.117 \le l_p \le 2 \text{ mm}$	0.76 mm	0.68 mm
Liquid thermal conductivity	$0.059 \le \hat{k}_l \le 0.0887 \text{ W/m-K}$	0.078 W/m-K	0.012 W/m-K
Latent heat of vaporization	$88 \leq \Delta h_{fg} \leq 222 \text{ kJ/kg}$	177 kJ/kg	0.899 kJ/kg
Specific heat capacity	$1103 \le c_p \le 1554 \text{ J/kg-K}$	1233 J/kg-K	146 J/kg-K
Absolute pressure	$0.1013 \le p \le 1.3 \text{ MPa}$	0.316 MPa	0.4 MPa
Surface tension	$4.35 \le \sigma_l \le 17.3 \text{ mN/m}$	13 mN/m	4.8 mN/m
Wall superheat	$0.26 \leq \Delta T \leq 26.64 \text{ K}$	9.3 K	7.58 K
Pore/fin pitch	$0.46 \leq L_p \leq 5 \text{ mm}$	2.17 mm	1.5 mm
Temperature	-6 ≤ <i>T</i> ≤ 49 °C	30 °C	14.9 °C
Heat flux	$1.18 \le q \le 429 \text{ kW/m}^2$	$85 \text{ kW/m}^2$	79 kW/m <sup>2</sup>

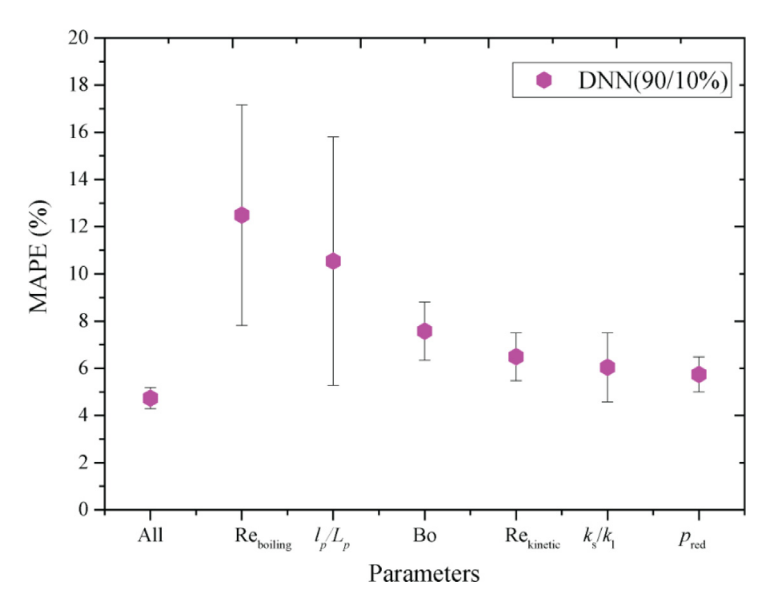


Fig. 12. Predicted MAPE of DNN excluding each designated input parameter, comparing with all parameters used, i.e., permutation-based sensitivity analysis. The error bars and train-test ratio are also shown.

atures, -6, 0, and 10°C using a new low-GWP refrigerant R1234ze. The pre-trained DNN predicts the experimental data within  $\pm 30\%$  error without additional DNN training with the data on R-1234ze, resulting in only MAPE = 17%. Fig. 11(b) compares the experimental measured HTC and predicted HTC of Pastuszko et al. [34]. The DNN predicts 70% of the data within  $\pm 30\%$ , leading to the MAPE of 27%. Also, Fig. 11(c) shows the predictions of DNN on the data of Yang and Fan [75] for the structured tubes during the boiling of R404A. The pre-trained DNN successfully predicts the 60% of the data within  $\pm 30\%$ , showing the MAPE of 26%. Details of the unseen (not used for DNN model training) dataset tested on the pre-trained model are given in Tables 5 and 6.

#### 3.4. Input parameter sensitivity on DNN model accuracy

In this section, the input parameter sensitivity on the DNN model accuracy is investigated by ignoring each input parameter based on the permutation method. The average MAPE of five different test runs with error bars is shown in Fig. 12 to compare with the one including all the input parameters, i.e., 4.7% MAPE.

The MAPE ignoring  $Re_{boiling}$  in the model results in the 12.49% average MAPE, which is nearly 2.5 times higher than that of the model including all the parameters. This large sensitivity of the Re<sub>boiling</sub> parameter is related to the fact that it includes the key geometrical, thermophysical, and operating parameters such as the heat flux q, pore size/fin spacing at the tip  $l_p$ , dynamic viscosity  $\mu_l$  and heat of vaporization  $\Delta h_{lg}$ . The second most sensitive parameter is the ratio of pore diameter or groove mouth spacing  $l_p$ to pore pitch  $L_p$  since the DNN prediction excluding  $l_p/L_p$  results in the 10.54% average MAPE, and this indicates the MAPE nearly doubles compared to the DNN prediction with all the input parameters. The large sensitivity results from the dominating geometrical parameter controlling the bubble dynamics and nucleate site densities which is in line with the previous studies. For instance, Mondal and Kim [22] reported that the HTC increases with the increased pore diameter and/or decreased pore pitch owing to the larger bubble size and active nucleation sites, although the optimal pore diameter and pore pitch exist for certain heat flux and type of refrigerant [29,64]. The bond number Bo is the next sensitive parameter as the MAPE increases nearly 1.5 times increases

excluding the Bo in the DNN model. The kinetic Reynold number  $\mathrm{Re_{kinetic}}$ , the thermal conductivity ratio  $k_s/k_l$  are the next sensitive parameters, although the sensitive changes are minimal. The least sensitive parameter is the reduced pressure  $p_{red}$  as the MAPE increase only up to 5.74% excluding the reduced pressure in the DNN model.

#### 4. Conclusion

In this study, we examined the complex relations among four geometrical, nine thermophysical properties, and two operational conditions to accurately predict the HTC on enhanced surfaces such as porous, sub-tunnels, reentrant cavity, or fin geometries over flat plate and tube surfaces, by incorporated those parameters into six dimensionless numbers as input parameters. The total of 1256 experimental data points is used including 7 working fluids at different conditions for more than 20 porous and reentrant cavity surface types. The optimized DNN model was obtained by carefully tuning the hyperparameters, which predicts 93% of the HTC within  $\pm 10\%$  error and results in MAPE below 5%. The developed DNN model outperformed the prediction accuracy of the existing empirical correlations having  $\pm 5.04$  - 45.37% MAPE.

Following key conclusions were drawn:

- The developed DNN model increased the pool boiling HTC prediction accuracy by at least 20% in MAPE, compared to the existing HTC correlations.
- The developed DNN model was sensitive to the boiling Reynolds number  $Re_{boiling}$  and the ratio of fin spacing at the tip(or pore diameter) to the pore pitch/center to center fin spacing  $l_n/L_n$ .
- Regardless of the train-test ratio (60/40 to 90/10%), the developed DNN model accuracy was always better than the existing semi-analytical model [36].
- Uncertainty analysis unveiled that there is at least 4  $\sim$  5% uncertainty in the DNN predictions.
- Due to its simplicity, flexibility, and high prediction accuracy, the developed DNN model can be used over existing complex models and empirical correlations.
- This study focuses on the basic framework of the DNN model aiming at understanding the structural-thermophysical-operating relations in the pool boiling HTC on the enhanced surfaces with relatively small datasets. The prediction accuracy can be further improved by including additional existing and future experimental studies. Also, this work can be extended to other similar scientific and engineering problems such as pool boiling with the different operating condition (different surface orientation), flow boiling on the enhanced surfaces.

#### **Declaration of Competing Interest**

The authors declare that they have no known competing financial interests or personal relationships that could have appeared to influence the work reported in this paper.

## CRediT authorship contribution statement

**Sadaf Mehdi:** Methodology, Investigation, Software, Data curation, Writing – original draft. **Saideep Nannapaneni:** Methodology, Investigation, Software, Writing – review & editing. **Gisuk Hwang:** Conceptualization, Supervision, Funding acquisition, Writing – review & editing.

#### Acknowledgment

This work is financially supported by the National Science Foundation (NSF), Award No. OIA-1929187 and the Wichita State Uni-

versity Convergence Sciences Initiative Program. This work is also financially supported by the College of Engineering, Wichita State University.

#### References

- [1] S. Nukiyama, The maximum and minimum values of the heat Q transmitted from metal to boiling water under atmospheric pressure, Int. J. Heat Mass Transf. 9 (12) (1966) 1419–1433, doi:10.1016/0017-9310(66)90138-4.
- [2] G. Liang, I. Mudawar, Review of nanoscale boiling enhancement techniques and proposed systematic testing strategy to ensure cooling reliability and repeatability, Appl. Thermal Eng. 184 (2021), doi:10.1016/j.applthermaleng.2020. 115982.
- [3] G. Liang, I. Mudawar, Review of pool boiling enhancement by surface modification, Int. J. Heat Mass Transf. 128 (2019) 892–933, doi:10.1016/j. ijheatmasstransfer.2018.09.026.
- [4] S.M. Ammar, C.W. Park, Evaporation heat transfer characteristics of falling film in small diameter fabricated tubes of absorption refrigeration system: an experimental investigation, Int. J. Heat Mass Transf. 165 (2021) 120618.
- [5] R.L. Webb, The evolution of enhanced surface geometries for nucleate boiling, Heat Transf. Eng. 2 (3-4) (2007) 46-69, doi:10.1080/01457638108962760.
- [6] L. Lin, M.A. Kedzierski, Review of low-GWP refrigerant pool boiling heat transfer on enhanced surfaces, Int. J. Heat Mass Transf. 131 (2019) 1279–1303.
- [7] M. Borumand, G. Hwang, Enhanced pool boiling critical heat flux on tilted heating surfaces using columnar-post wicks, in: Proceedings of the ASME International Mechanical Engineering Congress and Exposition, 85673, American Society of Mechanical Engineers, 2021 V011T11A028.
- [8] S. Mehdi, A. Mondal, N.H. Kim, Pool boiling heat transfer of R-123 on pored surfaces, in: Proceedings of the Society of Air-conditioning and Refrigerating Engineers of Korea (SAREK), 2019, pp. 610–613.
- [9] A. Mondal, S. Mehdi, N.H. Kim, Pool boiling heat transfer of R-134a on pored surfaces, in: Proceedings of the Society of Air-conditioning and Refrigerating Engineers of Korea (SAREK), 2018, pp. 453–455.
- [10] M. Egbo, M. Borumand, Y. Nasersharifi, G. Hwang, Surface orientation effects on pool-boiling with plain and enhanced surfaces, Appl. Thermal Eng. 204 (2021) 117927, doi:10.1016/j.applthermaleng.2021.117927.
- [11] R. Pastuszko, R. Kaniowski, T.M. Wójcik, Comparison of pool boiling performance for plain micro-fins and micro-fins with a porous layer, Appl. Thermal Eng. 166 (2020), doi:10.1016/j.applthermaleng.2019.114658.
- [12] S. Kotthoff, D. Gorenflo, E. Danger, A. Luke, Heat transfer and bubble formation in pool boiling: effect of basic surface modifications for heat transfer enhancement, Int. J. Thermal Sci. 45 (3) (2006) 217–236, doi:10.1016/j.ijthermalsci. 2005.01.011.
- [13] R.L. Webb, N. Kim, Enhanced Heat Transfer, Taylor and Francis, NY, 2005.
- [14] T.D.W. Nakayama, T. Nakajima, Effects of pore diameters and system pressure on saturated pool nucleate boiling heat transfer from porous surfaces, J. Heat Transf. (6) (1982) [Online]. Available:, doi:10.1115/1.3245085.
- [15] R.L. Webb, C. Pais, Nucleate pool boiling data for five refrigerants on plain, integral-fin and enhanced tube geometries, Int. J. Heat Mass Transf. 35 (8) (1992) 1893–1904
- [16] L.H. Chien, R.L. Webb, Visualization of pool boiling on enhanced surfaces, Exp. Thermal Fluid Sci. 16 (4) (1998) 332–341.
- [17] L.H. Chien, R.L. Webb, Measurement of bubble dynamics on an enhanced boiling surface, Exp. Thermal Fluid Sci. 16 (3) (1998) 177–186.
- [18] M. Kedzierski, L. Lin, Pool boiling of R514Å, R1224 yd (Z), and R1336mzz (E) on a reentrant cavity surface, J. Heat Transf. 143 (5) (2021).
- [19] J.R. Thome, Enhanced Boiling Heat Transfer, Hemisphere Pub. Corp.(Taylor & Francis), 1990.
- [20] Y. Wang, Z. Ma, J. Zhang, Pool boiling heat transfer on a reentrant cavity tube with R134a: effects of saturation temperature under ice storage condition, Int. J. Heat Mass Transf. 166 (2021), doi:10.1016/j.ijheatmasstransfer.2020.120762.
- [21] S. Mehdi, Y. Shah, A. Mondal, N.H. Kim, Bubble dynamics of R-134a boiling in enhanced surfaces having pores on sub-tunnels, Int. J. Heat Mass Transf. 155 (2020), doi:10.1016/j.ijheatmasstransfer.2020.119753.
- [22] A. Mondal, N.H. Kim, Nucleate pool boiling of R-134a on enhanced horizontal surfaces having pores on sub-tunnels, J. Enhanc. Heat Transf. 26 (3) (2019) 195–216, doi:10.1615/[EnhHeatTransf.2019028532.
- [23] R.L. Webb, Donald Q. Kern lecture award paper: odyssey of the enhanced boiling surface, J. Heat Transf. 126 (6) (2004) 1051–1059, doi:10.1115/1.1834615.
- [24] S.I. Haider, R.L. Webb, A transient micro-convection model of nucleate pool boiling, Int. J. Heat Mass Transf. 40 (15) (1997) 3675–3688.
- [25] U. Sajjad, et al., Determining the factors affecting the boiling heat transfer coefficient of sintered coated porous surfaces, Sustainability 13 (22) (2021) 12631.
- [26] Nakayama, W., Daikoku, T., Kuwahara, H., and Nakajima, T. "Dynamic Model of Enhanced Boiling Heat Transfer on Porous Surfaces—Part I: Experimental Investigation." ASME. J. Heat Transfer. 102(3)(1980): 445–450. doi:10.1115/1. 3244320.
- [27] Nakayama, W., Daikoku, T., Kuwahara, H., and Nakajima, T. "Dynamic Model of Enhanced Boiling Heat Transfer on Porous Surfaces—Part II: Analytical Modeling." ASME. J. Heat Transfer. 102(3)(1980): 451–456. doi:10.1115/1.3244321.
- [28] L.H. Chien, R.L. Webb, A nucleate boiling model for structured enhanced surfaces, Int. J. Heat Mass Transf. 41 (14) (1998) 2183–2195.
- [29] N.H. Kim, K.K. Choi, Nucleate pool boiling on structured enhanced tubes having pores with connecting gaps, Int. J. Heat Mass Transf. 44 (1) (2001) 17–28.

- [30] C. Ramaswamy, Y. Joshi, W. Nakayama, W.B. Johnson, Semi-analytical model for boiling from enhanced structures, Int. J. Heat Mass Transf. 46 (22) (2003) 4257–4269, doi:10.1016/s0017-9310(03)00216-3.
- [31] R. Pastuszko, Pool boiling for extended surfaces with narrow tunnels-visualization and a simplified model, Exp. Thermal Fluid Sci. 38 (2012)
- [32] R. Pastuszko, Pool boiling on micro-fin array with wire mesh structures, Int. J. Thermal Sci. 49 (12) (2010) 2289–2298.
- [33] R. Pastuszko, Boiling heat transfer enhancement in subsurface horizontal and vertical tunnels, Exp. Thermal Fluid Sci. 32 (8) (2008) 1564–1577.
- [34] R. Pastuszko, R. Kaniowski, N. Dadas, M. Bedla-Pawlusek, Pool boiling enhancement and a method of bubble diameter determination on surfaces with deep minichannels, Int. J. Heat Mass Transf. 179 (2021), doi:10.1016/j.ijheatmasstransfer.2021.121713.
- [35] R. Pastuszko, R. Kaniowski, T.M. Wójcik, Comparison of pool boiling performance for plain micro-fins and micro-fins with a porous layer, Appl. Thermal Eng. 166 (2020) 114658.
- [36] R. Pastuszko, T.M. Wójcik, Experimental investigations and a simplified model for pool boiling on micro-fins with sintered perforated foil, Exp. Thermal Fluid Sci. 63 (2015) 34–44
- [37] M.A. Kedzierski, L. Lin, Pool boiling of R515A, R1234ze(E), and R1233zd(E) on a reentrant cavity surface, Int. J. Heat Mass Transf. 161 (2020), doi:10.1016/j. iiheatmasstransfer.2020.120252.
- [38] A. Berber, M. Gürdal, K. Bağırsakçı, Prediction of heat transfer in a circular tube with aluminum and Cr-Ni alloy pins using artificial neural network, Exp. Heat Transf. 34 (6) (2020) 547–563, doi:10.1080/08916152.2020.1793826.
- [39] Y. Qiu, D. Garg, L. Zhou, C.R. Kharangate, S.M. Kim, I. Mudawar, An artificial neural network model to predict mini/micro-channels saturated flow boiling heat transfer coefficient based on universal consolidated data, Int. J. Heat Mass Transf. 149 (2020), doi:10.1016/j.ijheatmasstransfer.2019.119211.
- [40] L. Zhou, D. Garg, Y. Qiu, S.-M. Kim, I. Mudawar, C.R. Kharangate, Machine learning algorithms to predict flow condensation heat transfer coefficient in mini/micro-channel utilizing universal data, Int. J. Heat Mass Transf. 162 (2020), doi:10.1016/j.ijheatmasstransfer.2020.120351.
- [41] Z.E. Mohamed, Using the artificial neural networks for prediction and validating solar radiation, J. Egypt. Math. Soc. 27 (1) (2019), doi:10.1186/s42787-019-0043-8.
- [42] M. Balcilar, A.S. Dalkilic, A. Suriyawong, T. Yiamsawas, and S. Wongwises, "Investigation of pool boiling of nanofluids using artificial neural networks and correlation development techniques," Int. Commun. Heat Mass Transf., vol. 39, no. 3, pp. 424–431, 2012, doi:10.1016/j.icheatmasstransfer.2012.
- [43] M. Balcilar, A.S. Dalkilic, and S. Wongwises, "Artificial neural network techniques for the determination of condensation heat transfer characteristics during downward annular flow of R134a inside a vertical smooth tube," Int. Commun. Heat Mass Transf., vol. 38, no. 1, pp. 75–84, 2011, doi:10.1016/j.icheatmasstransfer.2010.10.009.
- [44] U. Sajjad, I. Hussain, K. Hamid, S.A. Bhat, H.M. Ali, C.C. Wang, A deep learning method for estimating the boiling heat transfer coefficient of porous surfaces, J. Thermal Anal. Calorim. 145 (4) (2021) 1911–1923.
- [45] U. Sajjad, I. Hussain, C.C. Wang, A high-fidelity approach to correlate the nucleate pool boiling data of roughened surfaces, Int. J. Multiph. Flow 142 (2021), doi:10.1016/j.ijmultiphaseflow.2021.103719.
- [46] Y. Shah, N.H. Kim, Bubble dynamics of R-134a/POE and R-123/MO mixture on enhanced surfaces having pores on sub-tunnels, Int. J. Heat Mass Transf. 184 (2022) 122258.
- [47] Y. Shah, C.H. Kim, N.H. Kim, Pool boiling of R-134A/polyolester oil lubricant mixtures on enhanced surfaces having pores, J. Enhanc. Heat Transf. 28 (8) (2021) 67–82, doi:10.1615/JEnhHeatTransf.2021039476.
- [48] Y. Shah, N.H. Kim, Pool boiling of R-123/MO and R-134a/POE lubricant mix-tures on pored surfaces, J. Mech. Sci. Technol. 36 (1) (2022) 467–478.
- [49] M. Cooper, Heat flow rates in saturated nucleate pool boiling-a wide-ranging examination using reduced properties, in: Advances in Heat Transfer, 16, Elsevier, 1984, pp. 157–239.
- [50] Mikic, B. B., and Rohsenow, W. M. "A New Correlation of Pool-Boiling Data Including the Effect of Heating Surface Characteristics." ASME. J. Heat Transfer.91(2)(1969): 245–250. doi:10.1115/1.3580136

- [51] S. Mehdi, N.H. Kim, Nucleate pool boiling of R-123 on pored surfaces, J. Enhanc. Heat Transf. 27 (7) (2020) 629–642, doi:10.1615/JEnhHeatTransf. 2020035147.
- [52] Y. Jiang, Y. Yu, J. Huang, W. Cai, J. Marco, Li-ion battery temperature estimation based on recurrent neural networks, Sci. China Technol. Sci. 64 (6) (2021) 1335–1344.
- [53] F. Nie, H. Wang, Q. Song, Y. Zhao, J. Shen, M. Gong, Image identification for two-phase flow patterns based on CNN algorithms, Int. J. Multiph. Flow 152 (2022) 104067, doi:10.1016/j.ijmultiphaseflow.2022.104067.
- [54] I. Goodfellow, Y. Bengio, A. Courville, Deep Learning, MIT Press, 2016.
- [55] U. Sajjad, I. Hussain, K. Hamid, H.M. Ali, C.C. Wang, W.-M. Yan, Liquid-to-vapor phase change heat transfer evaluation and parameter sensitivity analysis of nanoporous surface coatings, Int. J. Heat Mass Transf. 194 (2022), doi:10.1016/j.ijheatmasstransfer.2022.123088.
- [56] A. Géron, Hands-on Machine Learning with Scikit-Learn, Keras, and Tensor-Flow: Concepts, Tools, and Techniques to Build Intelligent Systems, O'Reilly Media, Inc., 2019.
- [57] G. Van Rossum, Fred L. Drake, Python 3 Reference Manual, CreateSpace, Scotts Valley, CA, 2009. ISBN 1441412697. Python, https://www.python.org.
- [58] F Pedregosa, G Varoquaux, A Gramfort, V Michel, B Thirion, O Grisel, M Blondel, P Prettenhofer, R Weiss, V Dubourg, J Vanderplas, et al., "Scikit-learn: Machine learning in Python." the Journal of machine Learning research, 12(2011),2825-2830. https://www.jmlr.org/papers/volume12/pedregosa11a/pedregosa11a.pdf.
- [59] François Chollet, keras, 2015. https://github.com/fchollet/keras.
- [60] John D Hunter, "Matplotlib: A 2D graphics environment.", Computing in science & engineering 09 (03) (2007) 90-95, doi:10.1109/MCSE.2007.55.
- [61] W. McKinney, Data structures for statistical computing in python (Vol. 445, No. 1, (2010, June) 51–56.
- [62] ML. Waskom, Seaborn, Statistical data visualization, Journal of Open Source Software 6 (2021) 3021, doi:10.21105/joss.03021.
- [63] Y. Tang, J. Zeng, S. Zhang, C. Chen, J. Chen, Effect of structural parameters on pool boiling heat transfer for porous interconnected microchannel nets, Int. J. Heat Mass Transf. 93 (2016) 906–917.
- [64] L.H. Chien, R.L. Webb, A parametric study of nucleate boiling on structured surfaces, part II: effect of pore diameter and pore pitch, J. Heat Transf. 120 (4) (1998) 1049–1054, doi:10.1115/1.2825889.
- [65] N.H.K. Ralph, L. Webb, Principles of Enhanced Heat Transfer, 2nd ed., Taylor & Francis. 2005.
- [66] S. Mehdi, Y. Shah, N.H. Kim, Bubble dynamics of R-123 and R-134a on pore/sub-tunnel surfaces, Int. J. Thermal Sci. 177 (2022) 107543.
- [67] S. Dahariya, N. Patel, M.K. Egbo, G. Hwang, A.R. Betz, High-pressure pool-boiling heat transfer enhancement mechanism on sintered-particle wick surface, Front. Mech. Eng. 5 (2020), doi:10.3389/fmech.2019.00071.
- [68] "Pandas correlation method documentation." https://pandas.pydata.org/pandas-docs/stable/reference/api/pandas.DataFrame.corr.html.
- [69] F. Pedregosa, et al., Scikit-learn: machine learning in Python, J. Mach. Learn. Res. 12 (2011) 2825–2830.
- [70] N. Srivastava, G. Hinton, A. Krizhevsky, I. Sutskever, R. Salakhutdinov, Dropout: a simple way to prevent neural networks from overfitting, J. Mach. Learn. Res. 15 (1) (2014) 1929–1958.
- [71] Kingma, D.P. and Ba, J., "Adam: A method for stochastic optimization". 2014. arXiv preprint arXiv:1412.6980.
- [72] N.K. Manaswi, Understanding and working with keras, in: Deep Learning with Applications Using Python, Springer, 2018, pp. 31–43.
- [73] Chien, L., and Webb, R. L. "A Parametric Study of Nucleate Boiling on Structured Surfaces, Part I: Effect of Tunnel Dimensions." ASME. J. Heat Transfer.120(4)(1998): 1042–1048. doi:10.1115/1.2825888
- [74] A. Kumar, C.C. Wang, Nucleate pool boiling heat transfer of R-1234ze (E) and R-134a on GEWA-B5H and smooth tube with the influence of POE oil, Appl. Thermal Eng. 201 (2022) 117779.
- [75] C.Y. Yang, C.F. Fan, Pool boiling of refrigerants R-134a and R-404A on porous and structured tubes part II. Heat transfer performance, J. Enhanc. Heat Transf. 13 (1) (2006) 85–97, doi:10.1615/JEnhHeatTransf.v13.i1.60.
- [76] T. Li, X. Wu, Q. Ma, Pool boiling heat transfer of R141b on surfaces covered copper foam with circular-shaped channels, Exp. Thermal Fluid Sci. 105 (2019) 136–143, doi:10.1016/j.expthermflusci.2019.03.015.